

DESIGN OPTIMIZATION OF A PIEZOELECTRIC ENERGY HARVESTING TEST RIG WITH SWIRLING AIR FLOW

Antiopi-Malvina Stamatellou*, Anestis I. Kalfas

* astamatel@auth.gr

Laboratory of Fluid Mechanics and Turbomachinery, Mechanical Engineering Department, Aristotle University of Thessaloniki, Thessaloniki, 54124, Greece

Keywords: Energy harvesting; piezoelectric film transducer; swirling flow; vibration

ABSTRACT

This paper presents an investigation of the energy harvesting potential of swirling air flows using commercial piezoelectric film transducers. Two test rigs were assembled and two main types of measurements were carried out on each one. First, an experimental set up comprising a centrifugal fan with an air swirler mounted at its exit was assembled. Pressure and piezo-transducer output voltage measurements were carried out for various fan speeds and the signals were processed with FFT. These were followed by energy harvesting tests which resulted in higher power outputs at lower fan speeds (maximum power 8.8 μ W). Experience from these experiments led to the design of a second test rig that employed a low power axial fan installed on a vibration absorbing base to produce the swirling flow. The maximum power harvested with the second set up was 0.15 μ W. Signals with higher rms voltages were produced with test rig B, which, however, were not associated with higher energy harvesting rates. Work is on-going to differentiate between the modes of electricity production of the two different sources of transducer excitation (beam flexure and chassis vibration).

Introduction

Energy harvesting from vibrations and flow turbulence is gaining increasing interest as a technology to replace battery use for powering microsystems located in remote places. Energy harvesters are reliable, environmentally friendly and need much less maintenance than batteries [1]. Experimental works in this field have been mostly carried out in wind tunnels using either bluff bodies [2] or grids [3] to produce flow induced vibrations. Turbulent flows transfer kinetic energy over a range of temporal and spatial scales and they can interact favorably with thin immersed piezoelectric beam elements producing electrical charge [4]. These devices can be tuned to the prevailing turbulence frequencies to produce maximum power output. The tuning mechanism has been well documented and explained in [5] as the resonance of the harvester with the energy source is critical in harvesting higher power output. The eigenfrequency of piezoelectric beams can be modified by changing their stiffness and length and adding tip masses. In the existing bibliography mean flow velocities are not widely varied inside the tunnels and the same is true for the resulting prevailing frequencies of turbulence. Since the transducer's oscillation frequency affects the harvester's performance, it is interesting to investigate the transducer's response to a wide variety of excitation frequencies. One recent approach in the design process of beam type transducers is the bi-stable piezoelectric energy harvester [6] that allowed fixing of the piezoelectric beam's eigenfrequency. Other realized concepts of energy harvesters studied include the 'piezoelectric grass' [7], with PZT piezoelectric film element arrays arranged perpendicular to the flow direction, producing about 1 μ W at a mean velocity of 11 m/s, or the placement of two tandem piezoelectric harvesters in smooth flow conditions [8]. Other

studies have attempted to exploit the air flow energy inside heating, ventilation, and air conditioning (HVAC) systems [9], the harvesting potential of energy from footsteps by installing piezoelectric tiles in a library building [10] and the installation of aero-elastic belts [11] on high points of buildings.

This paper summarizes experience from assessing the energy harvesting potential of swirling air flows using a commercial piezoelectric film transducer [12], which exploits both flow turbulence energy and chassis vibration energy. In that context, the authors have already presented results of an experimental set up comprising a centrifugal fan - air swirler arrangement [13]. A second test rig was constructed that was based on an axial fan with significantly reduced power. The results obtained are compared with those of the previous test rig and employed for better understanding of the harvester’s performance.

Experimental methods and test rigs

Commercial piezoelectric film patches (Measurement Specialties, LDT0-028K [12]) made from PVDF were employed in both test rigs (technical data in Table 1). The piezoelectric films were used as slender beams clamped at one end and free at the other. Following the example of other researchers [14, 15], it was confirmed that the addition of a plastic attachment with a similar Young’s modulus with the PVDF film [13] improves the harvester’s behavior. Attachments mounted on the piezoelectric film transducers of both test rigs (Figure 1) resulted in higher voltage rms values and power outputs.

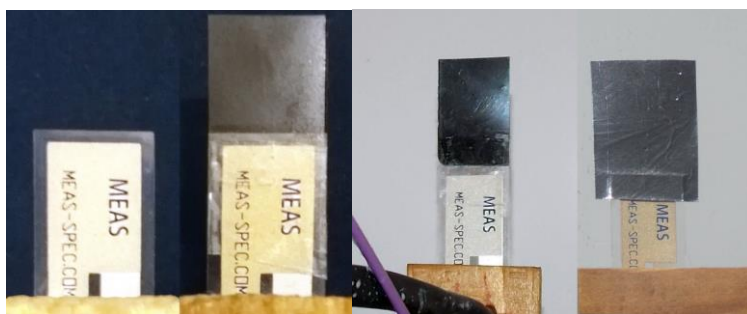


Figure 1 Two transducer configurations of different lengths employed in test rig A (left), another two in test rig B (right)

Table 1 Piezo-film transducer properties [12]

PVDF Transducer properties		
Elastic modulus	3	GPa
Density (PVDF)	1780	kg/m ³
Piezoelectric coupling	0.07	C/m ²
Beam length	22	mm
Beam width	13	mm
Beam thickness	0.2	mm
Substrate material	mylar	

In test rig A [13], the turbulent flow was created by a centrifugal fan –swirler plate arrangement (Figure 2a). The air flow field created had a Reynolds number of 15.000-130.000 and a swirl number of 0.3-0.4. The transducer was fixed to a solid base with outlets for the two sensor wires. The mounting mode of the transducer allowed for varying its position and orientation, to optimize energy harvesting. The transducer’s output was connected to a power regulating circuit and the average power output was monitored by measuring the circuit’s output voltage across a load resistance. The static

pressure and transducer’s output signals were recorded for various fan speeds and transducer’s orientations.

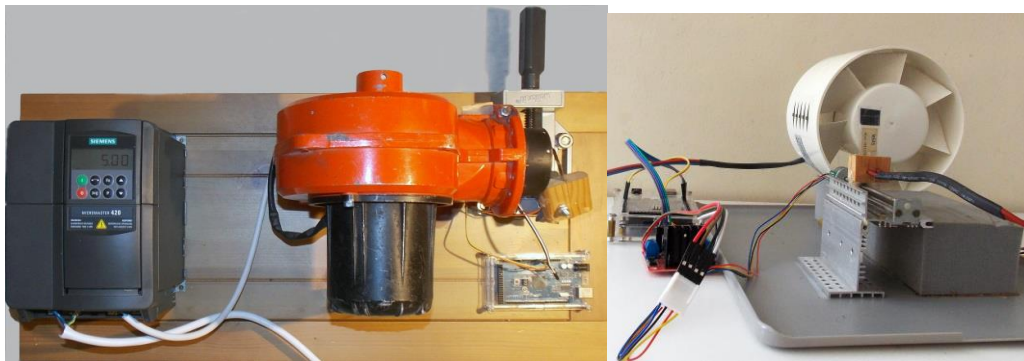


Figure 2 (a) Test rig A – Inverter, centrifugal fan-swirler plate, piezo-film transducer (b) Test rig B - axial fan, piezo-film transducer, traversing mechanism

Test rig B (Figure 2b) comprised a low-power axial fan (20 W at the maximum speed of 2100 rpm) installed on a polyurethane foam vibration absorbing base in order to avoid transmission of chassis vibrations and a traversing mechanism to control the axial position of the piezoelectric beam in relation to the fan’s exit. The fan’s motor speed was controlled using a PWM voltage regulator (50-250V). The radial position of the transducer was kept constant, after an initial optimization phase (Figure 2b). The mean flow velocity produced was between 0.7 and 7 m/s and the Reynolds number ranged at 5,000 - 50,000. The maximum swirl number measured was 0.4. The transducer was clamped to a base with outlets for the two sensor wires. The base was mounted to a linear motion mechanism controlled with a 2-phase DC stepper motor, controlled by an Arduino MEGA 2560 board. A 16-bit 400 kSa/s Data Acquisition Board was employed for the voltage output and harvesting time cycle measurements.

Table 2 Main geometrical and mechanical property data for the piezo-film transducers employed

Designation	Description/ sensor type	Test rig	Total Length [mm]	Width b [mm]	Thickness h [mm]	Density (mylar) [kg/m ³]
#0	Standard PVDF transducer without attachment	A	22 mm	13	0.2	1390
#1	PVDF transducer w 15x13 mm attachment	A	37 mm	13	0.2	1390
#2	PVDF transducer w 20x20 mm soft plastic attachment	B	42 mm	13-20	0.2	1390
#3	PVDF transducer with 13x20 mm attachment	B	42 mm	13	0.2	1390

Voltage output and energy harvesting measurements

In test rig A, the static pressure and piezo-film transducer’s output signals were recorded simultaneously for various fan speeds to investigate the relation of the harvester’s voltage output with the pressure signal measured with a piezo-resistive sensor. FFT was performed at the two signals and a good agreement was discovered between their main frequencies (Fig.3b). It was also found that the output voltage rms value displayed a steady decrease with the increase of the mean flow velocity both of the piezo-film’s configurations. The same was true for the energy harvesting time cycle of the

piezo-film transducers, which is the time needed to charge the input capacitor up to a certain voltage. The harvesting time cycle, which is indicative of the harvested power levels, is lower at lower fan flow rates. The higher power output of test rig A was displayed at 6 Hz Inverter’s frequency that translated to 12% of the centrifugal fan’s maximum power. The test matrix is presented in Table 3.

A voltage rectifying circuit board (LTC3588-1) was used to regulate the voltage output of the piezoelectric energy harvester. At the inlet side of the board, a 22 μF capacitor or alternatively, a 4.7 μF capacitor was connected. At the outlet a 47 μF capacitor in parallel with a 150 Ω resistance were connected. This low-loss full-wave bridge rectifying board also helps in the storage of charge in the input capacitor until a lockout voltage is reached and then transfers a portion of the stored charge to the output load (150 Ohm resistor). The average power output was monitored by measuring the voltage across a load resistance connected with the rectifying circuit board. The voltage measurements were taken at the input and output capacitors by connecting the NI Data acquisition board and a PC running MATLAB - Data Acquisition Toolbox [16]. Measurements were performed at different fan speeds and different axial distances of the film transducer from the fan’s exit, to study the time cycle of the energy harvesting process. The sampling rate was at 1 kSa/s.

A similar set of measurements was performed for test rig B. The fan speed and the distance from the fan’s exit were varied and the measurements’ details are presented in the test matrix (Table 3).

Table 3 Test matrix for the voltage output (x) and energy harvesting (x) measurements of test rig B

Fan speed [rpm]	600	1000	1700	2100
Transducer distance from fan’s exit [mm]				
65	x	x	x	x
80	x	x	x	x
95	x	x	x	x
110	x	x	x	x

Results and discussion

In order to better understand the behavior of the transducer, a typical period of 1 second was extracted from each recording and is comparatively presented in Figure 13 for 3 fan speeds and 3 axial positions of the transducer. The maximum amplitude range measured was ± 10 V. With test rig B, the amplitude range of the oscillator for a fan speed of 1000 rpm was about ± 2 V, for a speed of 1700 rpm ± 5 V and for a speed of 2100 rpm ± 10 V.

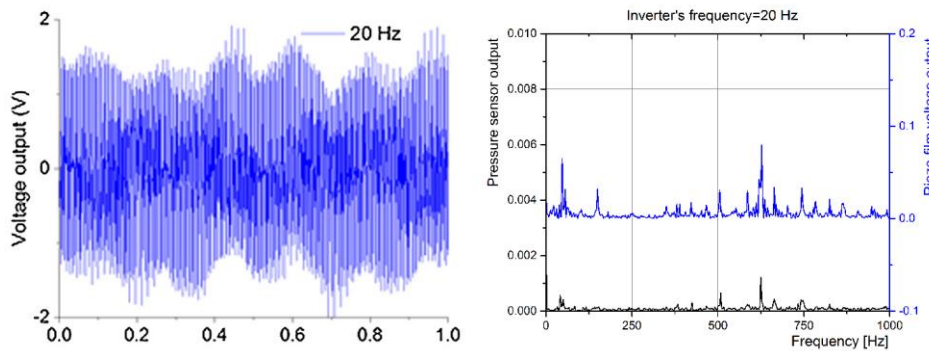


Figure 3 Test rig A (a) – Voltage output waveform for piezo-film configuration #1 (b) Power spectral densities of transducer’s voltage signals (FFT), inverter’s frequency=20 Hz

The period of oscillation of the electrical signal seems to stay more or less steady at about 40 Hz, whereas the amplitude of oscillations presents a modulation. The amplitude modulation may be explained by the fact that we have a forced oscillation produced by flow eddies of differing length and time scales that cause the forcing function to be in phase or out of phase with the beam's oscillation, thus increasing or decreasing its amplitude.

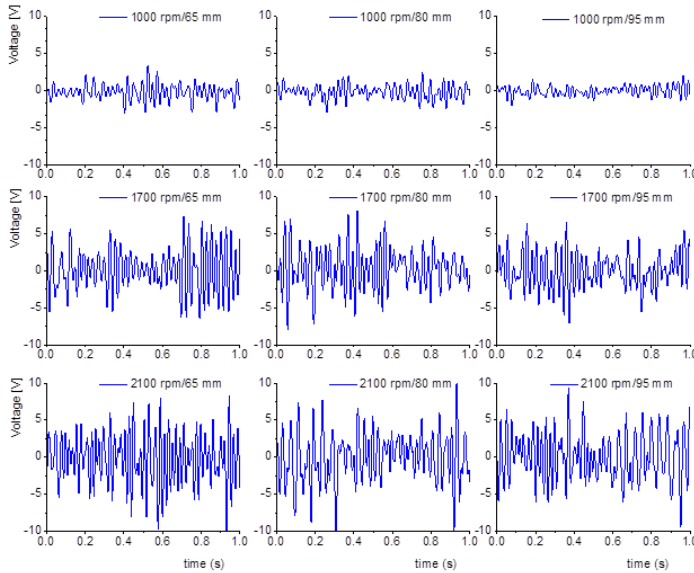


Figure 4 – Piezo-film #2 - plot of voltage output waveforms for various fan speeds and transducer positions

At test rig B for transducer #3, a period of 1 s was extracted from each recording and comparatively presented in Figure 4 for the same fan speeds and axial transducer positions. Transducer #3 demonstrated higher amplitude range and higher V_{rms} values. The period of signal oscillation stays more or less steady at about 40 Hz, however the amplitude modulation is more enhanced, with standard deviations comparatively presented in Figure 5. The amplitude effect may be explained by the film's extension being stiffer and its forcing effect on the beam's oscillation more effective. Despite the area of extension being bigger with transducer #2.

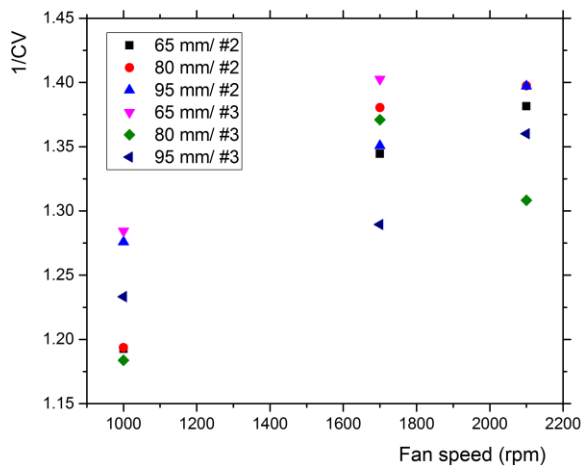


Figure 5 test rig B –ratio of standard deviation to mean (σ/μ) of voltage signal waveform amplitude modulation

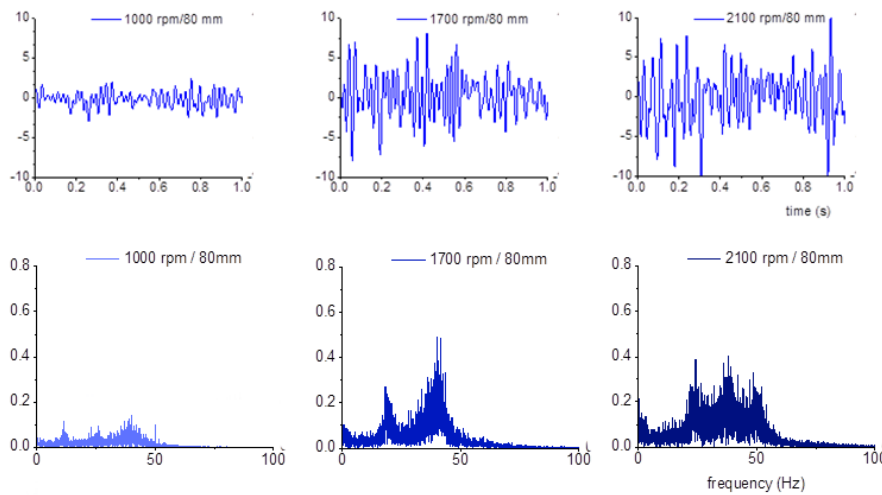


Figure 6 Test rig B (a) – Output voltage waveforms plot for transducer configuration #2 at 80 mm distance, for three different fan speeds (b) The respective power spectral densities for the same output voltage signals (FFT)

It is apparent from the spectral analysis of the voltage output signals that the eigenfrequency of the piezoelectric beam with configuration #2 is at 39.5 Hz, as there was a prominent peak in different fan speeds and distances from the fan’s exit presented in Figure 6b. This is in raw agreement with the approximate calculations for the first eigenfrequency of the beam, if one takes into account that the extension is only approximately equivalent to the transducer’s material in terms of density and Young’s modulus. Dominant frequencies of the voltage signal are observed at about 25 and 40 Hz. The dominant frequencies are not affected by the fan’s speed which is in line with the theory of forced vibrations. The dominant frequencies of the piezo-film are observed in the range of 0-60 Hz.

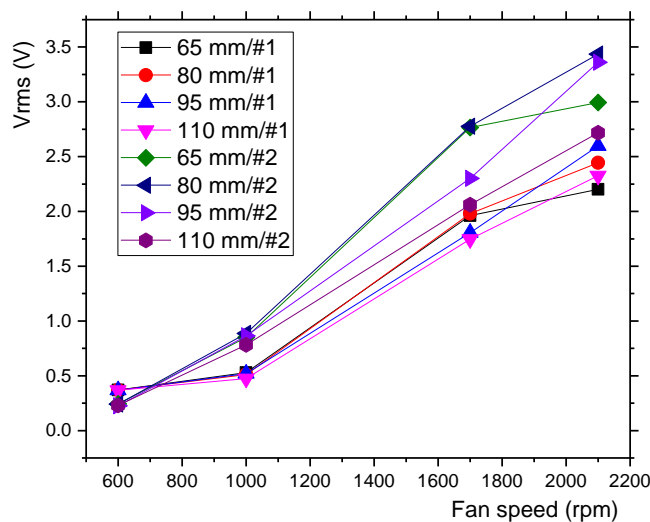


Figure 7 Transducer’s output voltage (rms) versus fan speed for the two versions of the piezo-film transducer at various distances from the fan’s exit (test rig B)

The voltage rms value is an indication of the power harvesting potential. It was observed (see Figure 7) that rms values of the transducer’s voltage output were higher with transducer #2. The most

favorable distances from the fan’s exit were found to be 0.73 and 0.86 fan diameters. The rms voltage value was higher with higher mean flow velocities. The highest rms voltage was observed at 2100 rpm fan speed for sensor #2 at 80 mm distance from the fan’s exit. The highest voltage rms value observed was 3.5 V while at the maximum fan speed the rms values were in the range of 2 V to 3.5 V. The rms values observed in the previous study were in the range of 0.4 V to 1.4 V [13]. A comparative diagram of the voltage rms value versus the Reynolds number is presented in Figure 8 for both setups.

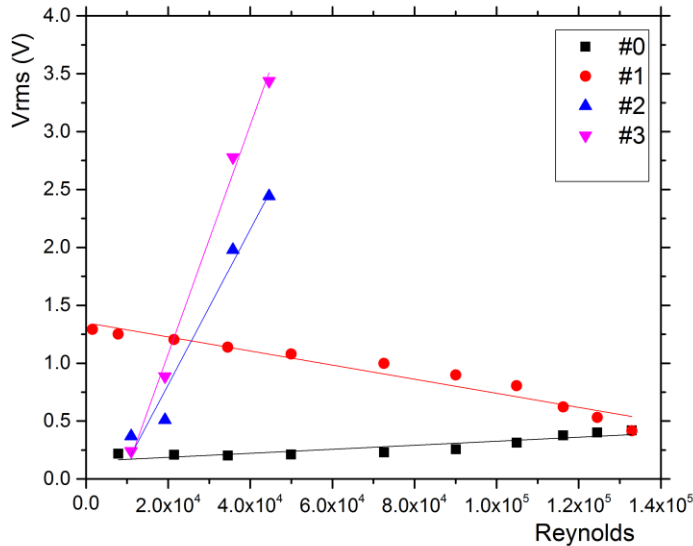


Figure 8 Transducer output voltage rms versus Reynolds numbers for all four configurations (test rig A & B)

Test rig B demonstrated significantly higher voltage rms values than test rig A with the maximum value at 3.5 V vs. 1.4 V for test rig A. It is an interesting observation that setup B, with a vibration damping base, the Vrms value was increasing with the increase of the Reynolds number, whereas in setup A the Vrms value decreased with the increase of the Re number as seen in Figure 8.

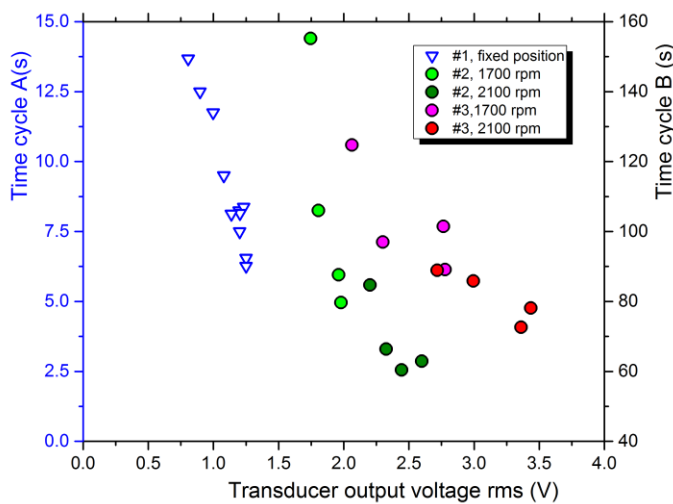


Figure 9 - Transducer output voltage rms versus harvesting time cycle. Comparison for both test rigs A & B

The investigation of the relationship between the voltage root mean square value and the harvesting time cycle was continued. This relation is plotted in Figure 9, for the two piezo-film configurations as well as for the one with the extension from the previous study [13] (#0), the increase of the voltage output rms value leads to the decrease of the harvesting time cycle. The harvesting time cycle of the configuration #0 was normalized to be comparable with the measurements with the current setup. The configuration #0 displayed better results, as the harvesting time cycle was shorter, despite the lower rms voltage values. It is concluded that the rms voltage is related with the power output of the energy harvester but it is not the only factor affecting it. However, for a specific set-up higher voltage rms produces lower harvesting time cycle. The frequency of the voltage output seems to have an impact at the charging of the capacitor, as the rms voltage is indicative of the energy carried by the signal.

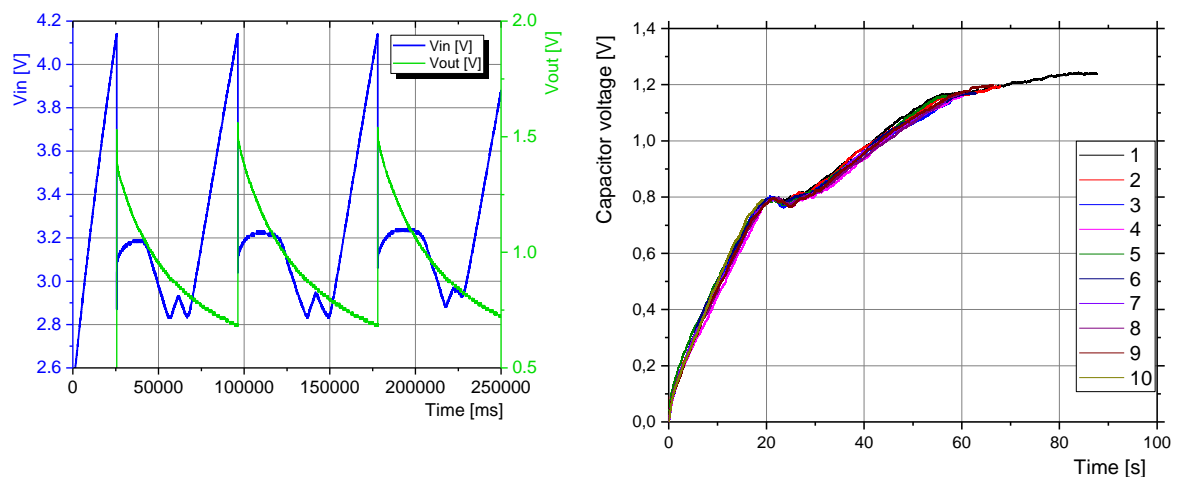


Figure 10 (a) Test rig A – Voltage at inlet and outlet capacitors during 3 successive time cycles (b) Test Rig B: Voltage increase at the inlet capacitor during ten consecutive harvesting time cycles (4.7 μ F, #1)

The power producing capacity of the transducers, with their output connected to a power regulating circuit and an external load was studied. In Figure 9 (b) the performance of the energy harvesting circuit is presented. The performance was monitored by measuring the voltage output at the 4.7 μ F input capacitor of the regulator board. The charging of the capacitor has a repeatable behavior. The measured voltage seen in Figure 10 (b) exhibited a local maximum point at 0.8 V followed by a local minimum point before it resumes charging to higher voltage. The measurements were performed at 2100 rpm and 95 mm distance from the fan which is the point with the highest voltage rms value. The sampling frequency of the experiment was 1 kHz. The capacitor was discharged after each collection cycle. The average power output of the harvester can be measured by measurement of the collection time up to a specified voltage, say 0.8 V or 1.2 V in Figure 10 (b). The harvesting time cycle's variation with the fan speed and the transducer's position is presented in Figure 11.

Two measurement sets were performed for the harvesting time cycle. A time cycle stands for the time the inlet capacitor takes to charge up to 0.8 V. This value was chosen based on the charging behavior of the capacitor demonstrated in Figure 10(a). The harvesting time cycles of the two sensors exhibited quite similar behaviors with the change of distance and fan speed. The minimum time cycle (maximum power), is observed at 0.73 and 0.86 fan diameters. This time interval is a measurement of the efficiency of the energy harvester as well as an important characteristic for the applications the harvester can be employed for.

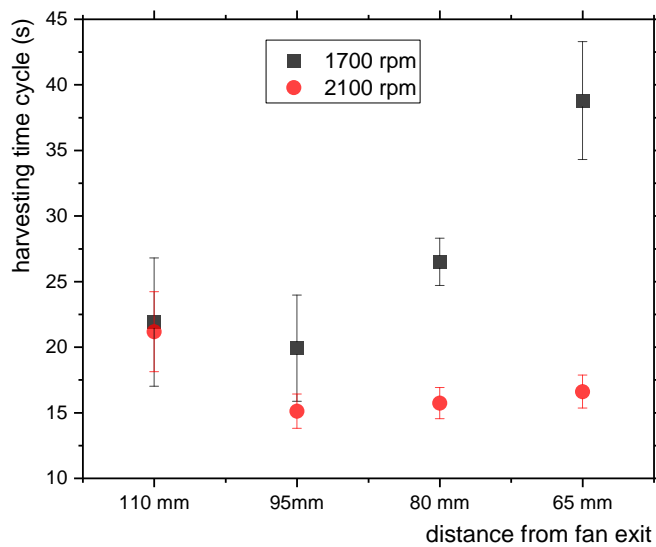


Figure 11 Test rig B - Energy harvesting time cycle vs. distance from fan's exit and fan speed (#1, 4.7 μF 16 V)

Measurements were performed to observe its variation with the inverter's frequency with the two types of piezo-film transducer (Figure 11). It is clear that the time cycle was smaller with the transducer type #2 where the attachment mounted on the beam was of equal stiffness to the transducer's material. The time cycles measured were in the range of 15 to 40 seconds using a 4.7 μF capacitor until its charge was up to 0.8 V. The best positions were observed to be at distances of 0.73 and 0.86 fan diameters. The harvesting time cycle was shorter with higher mean flow velocities. The electrical energy stored in the 4.7 μF input capacitor in each cycle (see Figure 11) is 2 μJ . Thus, the average power was estimated to be 0.15 μW at the optimum position and the highest fan speed.

Conclusions

Two test rigs were assembled and tested, the first (A) comprising a centrifugal fan with air swirler and the second (B) comprising an axial fan of low power input. The FFT transformations of the signals produced by the two test rigs, point to two different mechanisms of energy harvesting. It was discovered that the main electrical signal frequencies with test rig B were lower than 60 Hz and this is explained by the fan being installed on a vibration absorbing base. On the other hand, higher vibration frequencies were found in the FFT spectra of output of test rig A that were attributed to chassis vibration transferred from the fan to the transducer through the base. The particular type of piezo-film is known to be very sensitive to mechanical vibration frequencies around 150 Hz.

In test rig B higher Reynolds numbers produced higher voltage rms values. With test rig B it was possible to achieve higher rms voltage values (2-3.5 V) than with test rig A (0.4-1.4 V).

The high rms voltage values produced at test rig B were not translated to a higher power producing ability. With test rig B it was not possible to charge the regulator's inlet capacitor to more than 1.2 V, whereas with test rig A it was charged up to 3.8 V. The maximum harvested power was 8.8 μW with test rig A and 0.15 μW with test rig B. Work is on-going to differentiate between the effects of the two different sources of transducer excitation (beam flexure and chassis vibration) to the energy produced.

References

1. Toprak, A. and O. Tigli, *Piezoelectric energy harvesting: State-of-the-art and challenges*. Applied Physics Reviews, 2014. **1**(3): p. 031104.
2. Hu, Y., et al., *Modeling and experimental study of a piezoelectric energy harvester from vortex shedding-induced vibration*. Energy Conversion and Management, 2018. **162**: p. 145-158.
3. Danesh-Yazdi, A.H., N. Elvin, and Y. Andreopoulos, *Parametric analysis of fluidic energy harvesters in grid turbulence*. Journal of Intelligent Material Systems and Structures, 2016. **27**(20): p. 2757-2773.
4. Andreopoulos, Y., et al., *The Effects of Turbulence Length Scale on the Performance of Piezoelectric Harvesters*. 2015(57250): p. V002T22A005.
5. Naudascher, E. and D. Rockwell, *Flow-Induced Vibrations: An Engineering Guide*. 2012: Dover Publications.
6. Pan, D. and F. Dai, *Design and analysis of a broadband vibratory energy harvester using bi-stable piezoelectric composite laminate*. Energy Conversion and Management, 2018. **169**: p. 149-160.
7. Hobeck, J.D. and D.J. Inman, *Artificial piezoelectric grass for energy harvesting from turbulence-induced vibration*. Smart Materials and Structures, 2012. **21**(10): p. 105024.
8. McCarthy, J.M., et al., *On the visualisation of flow structures downstream of fluttering piezoelectric energy harvesters in a tandem configuration*. Experimental Thermal and Fluid Science, 2014. **57**: p. 407-419.
9. Petrini, F. and K. Gkoumas, *Piezoelectric energy harvesting from vortex shedding and galloping induced vibrations inside HVAC ducts*. Energy and Buildings, 2018. **158**: p. 371-383.
10. Li, X. and V. Strezov, *Modelling piezoelectric energy harvesting potential in an educational building*. Energy Conversion and Management, 2014. **85**: p. 435-442.
11. Aquino, A.I., J.K. Calautit, and B.R. Hughes, *Integration of aero-elastic belt into the built environment for low-energy wind harnessing: Current status and a case study*. Energy Conversion and Management, 2017. **149**: p. 830-850.
12. Measurement_Specialties, *LDT with Crimps Vibration Sensor/Switch Data Sheet*. 2008.
13. Stamatellou, A.-M. and A.I. Kalfas, *Experimental investigation of energy harvesting from swirling flows using a piezoelectric film transducer*. Energy Conversion and Management, 2018. **171**: p. 1405-1415.
14. Li, S. and H. Lipson, *Vertical-Stalk Flapping-Leaf Generator for Wind Energy Harvesting*. 2009(48975): p. 611-619.
15. Yang, Z., et al., *Introducing arc-shaped piezoelectric elements into energy harvesters*. Energy Conversion and Management, 2017. **148**: p. 260-266.
16. Mathworks. *MATLAB Overview*. 2018; Available from: <https://www.mathworks.com/products/matlab.html>.